Compact Mach–Zehnder Interferometer Ce:YIG/SOI Optical Isolators

Samir Ghosh, Shahram Keyvaninia, Yuya Shoji, Wim Van Roy, Tetsuya Mizumoto, Gunther Roelkens, and Roel G. Baets

***Abstract*— We demonstrate an optical isolator integrated with a silicon-on-insulator waveguide platform realized by the adhesive bonding of a Ce:YIG/SGGG die on top of a Mach–Zehnder interferometer (MZI). The design is based on the different nonreciprocal phase shifts (NRPS) experienced by both arms of the interferometer, which have different waveguide widths. Simulation of NRPS versus silicon waveguide width is shown for a few different benzocyclobutene bonding layer thicknesses for a particular silicon waveguide thickness and Ce:YIG/SGGG stack. Variations of NRPS as a function of MZI arm lengths with bonded stack on top of MZI are measured. Optical isolation of 11 dB is experimentally obtained for a device with a footprint of 1.5 mm × 4 μm.**

***Index Terms*— Benzocyclobutene bonding, Ce:YIG, isolator, silicon on-insulator (SOI).**

I. Introduction

In RECENT years many optical functions for optical communication systems have been realized on the silicon-on-insulator (SOI) waveguide platform. Also semiconductor laser diodes, which are of key importance in such systems, are being integrated on this platform [1]. Since the performance of a laser is very sensitive to back-reflections from other components in the circuit, an optical isolator is highly desired. Until now bulk isolators are serving this purpose but for a compact solution the co-integration of an isolator with a laser on the SOI platform is of paramount importance. To construct an optical isolator in linear, time-independent systems a nonreciprocal material is required. A magnetic material can show non-reciprocity in the presence of an external magnetic field. In bulk isolators a piece of YIG is kept between two polarizers with polarization axes offset by 45° and an external magnetic field is applied in the light propagation direction. This rotates the polarization of the incident light by 45° and by another 45° in the backward direction, thereby obtaining high optical isolation. Implementing this concept in a waveguide configuration has been assessed [2] but because of the particularly strong birefringence of SOI waveguides it puts stringent requirements on waveguide dimensions in order to obtain phase matching between the transverse electric (TE) and transverse magnetic (TM) mode. To avoid the need for phase-matching, instead of non-reciprocal polarization rotation, the non-reciprocal phase shift (NRPS) experienced by the TM polarized mode due to the presence of a lateral magnetic field is typically utilized in a waveguide configuration [3]. The nonreciprocal material can be bonded [4]–[6] or deposited [7] on top of the waveguide circuit to realize an optical isolator. Currently, the material quality of the deposited material is still inferior to the as-grown material. Therefore, in this letter we focus on the bonding of Ce:YIG/SGGG dies on a silicon waveguide circuit, for which an adhesive die-to-wafer bonding process is used using DVS-BCB as the bonding agent. Recently, Mach–Zehnder interferometer (MZI) [4], [6] and ring resonator structures [5], [7] have been demonstrated as an optical isolator. In [6], the garnet die needs to be aligned on top of the MZI arms in such a manner that light propagating in one arm experiences an opposite nonreciprocal phase shift compared to the other arm. To achieve this a separation of nearly 400 μm was designed between the garnet covered and the garnet-free part. In case of the MZI isolator demonstrated in [4] an anti-parallel magnetic field was required and consequently a separation of 400 μm between the two arms was needed to accommodate the external magnet. In [5] a large radius ring resonator was presented as an optical isolator. Again, the device radius was kept large to accommodate an external magnet. In this letter we present a new bonding-based optical isolator based on a MZI, which does not show any alignment issues and results in a compact device, since a unidirectional magnetic field is used covering the entire device.

II. Isolator Design

The conventional MZI-based isolators described in [4], [6] are constructed by connecting two multimode interferometer couplers by two silicon waveguides of identical width and work on the basis of the opposite NRPS experienced by TM light propagating through the garnet covered waveguides (push-pull operation). Our proposed device also consists of two multimode interferometers (MMI), which are however

Manuscript received June 12, 2012; revised August 3, 2012; accepted August 6, 2012. Date of publication August 8, 2012; date of current version August 29, 2012. This work was supported in part by the Methusalem Project "Smart Photonic ICs" of Ghent University and in part by the European Commission through the Project "Smartfiber."

S. Ghosh, S. Keyvaninia, G. Roelkens, and R. G. Baets are with the Department of Information Technology, Photonics Research Group, Ghent University-IMEC, Ghent 9000, Belgium (e-mail: samir.ghosh@intec.ugent.be; shahram.keyvaninia@intec.ugent.be; gunther.roelkens@intec.ugent.be; roel.baets@intec.ugent.be).

Y. Shoji and T. Mizumoto are with the Department of Electrical and Electronics Engineering, Tokyo Institute of Technology, Tokyo 152-8552, Japan (e-mail: shoji.y.ad@m.titech.ac.jp; tmizumot@pe.titech.ac.jp).

W. Van Roy is with IMEC, Leuven B-3001, Belgium (e-mail: vanroy@imec.be).

Color versions of one or more of the figures in this letter are available online at http://ieeexplore.ieee.org.

Digital Object Identifier 10.1109/LPT.2012.2212426

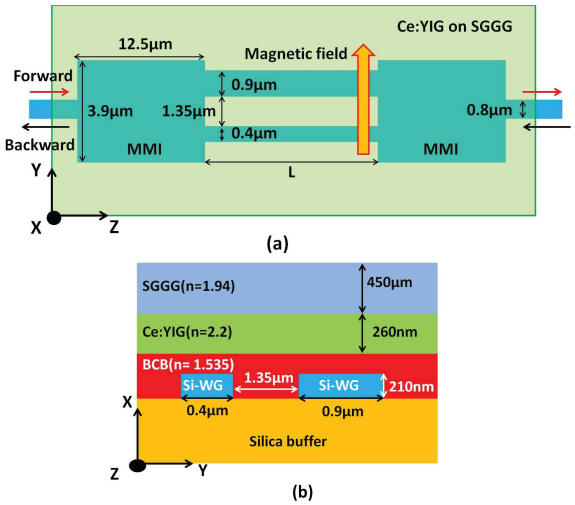

Fig. 1. Schematic of bonded isolator. (a) Top view. (b) Cross-sectional view.

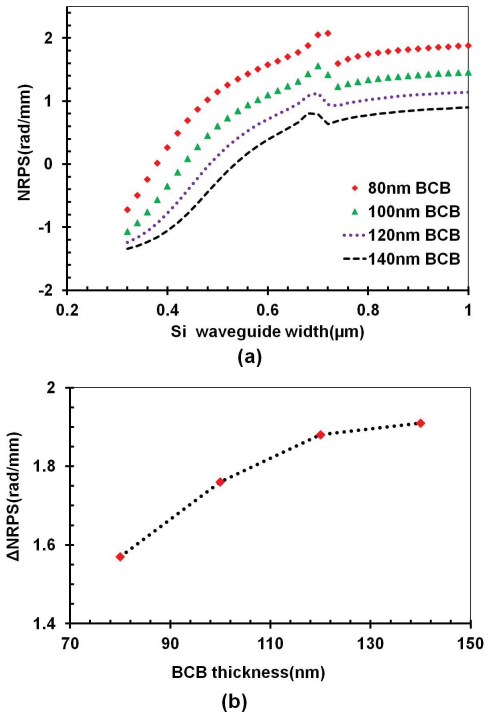

Fig. 2. (a) Simulation of NRPS per unit length versus waveguide width for different BCB layer thicknesses for a 260 nm thick Ce:YIG layer with a 210 nm thick Si waveguide. (b) Plot of the differential NRPS versus BCB thickness for waveguide widths of 0.4 and 0.9 μm.

connected by two silicon wire waveguides of different width. Since both waveguides have a different width, they experience a different NRPS in a unidirectional magnetic field oriented identically in both waveguides, and hence a net non-reciprocal phase shift between both arms can be achieved. The device layout is shown in Fig. 1(a) and Fig. 1(b). A similar approach using different cladding materials to induce a net non-reciprocal phase shift was presented in [8]. As can be seen, compact isolator structures can be realized this way. The MMIs are designed for having a bonded garnet layer on top. This relaxes the alignment requirements on the positioning of the Ce:YIG/SGGG dies, since the complete interferometer can be covered with the garnet. The length and width of the multimode section of the MMI are designed to be 12.5 μm and 3.9 μm, respectively in a 210 nm silicon waveguide layer geometry. The width of the input waveguide is 0.8 μm. The output waveguides of the MMI are 0.9 μm and 0.4 μm wide, respectively and the offset between them is designed as 1.35 μm. A ferrimagnetic 260 nm Ce:YIG layer on a SGGG substrate (450 μm) is bonded on top of the MZI as shown in Fig. 1(b). The NRPS per unit length is calculated by evaluating the perturbation formula [9], [10]

$$\mathrm{NRPS} = \frac{\int\int_{Ce:YIG} g(x,y)\varepsilon_0 \frac{\partial}{\partial x}\frac{|H_y|^2}{n^4} dxdy}{\iint \frac{1}{n^2}|H_y|^2 dxdy} \quad (1)$$

where H_y is the unperturbed transverse magnetic field distribution in the waveguide and $g(x,y) = n\lambda\theta_F/\pi$ is the magneto-optical constant of the Ce:YIG layer. θ_F is the specific Faraday rotation of the Ce:YIG ($\theta_F = -5000°$/cm at $\lambda = 1.5$ μm), and n is the refractive index of the same material. ε_0 is the vacuum permittivity. λ is the free-space wavelength of light propagating through the magnetic media. The transverse magnetic field component of the quasi-TM polarized mode is simulated by the finite element method (FEM) using full-vectorial eigenmode expansion software [11] for different waveguide widths and BCB thicknesses. The integration in the numerator is carried out for the whole waveguide cross-section whereas in the denominator it is limited to the magneto-optic Ce:YIG slab. The NRPS per unit length as a function of waveguide width for different BCB thicknesses is presented in Fig. 2(a) for a wavelength of 1500 nm with 210 nm Si core thickness. It is clear from Fig. 2(a) that the wider arm experiences a higher NRPS compared to the narrower arm. As a result a net differential NRPS (ΔNRPS) is obtained. It is important to mention here that the NRPS starts changing sign below a particular waveguide width for a given BCB thickness. This is because the H_y field at Ce:YIG/SGGG interface becomes larger than that of Ce:YIG/BCB interface for that waveguide width and BCB thickness. Discontinuity in Fig. 2(a) around waveguide width 0.7 μm is due to the mode coupling between the fundamental TM mode and a high-order TE mode.

For the specific case of 0.4 μm and 0.9 μm wide arms of the Mach–Zehnder interferometer, the differential NRPS is plotted in Fig. 2(b). The MMI used in the current design has two different output widths. This design is chosen over an MMI design with identical output waveguide widths and a taper section in one arm due to the fact that during the tapering between a 0.9 μm and 0.4 μm wide waveguide, a TM/TE mode anti-crossing, due to the vertical asymmetry in the layer stack, results in substantial power loss [12]. The power coupling efficiency to both output waveguides (at 1500 nm wavelength) of the MMI with unequal output widths (C_1^2 and C_2^2 are the power coupling efficiencies to the 900 nm wide and 400 nm wide waveguide, respectively) is shown in Fig. 3 as a function of BCB layer thickness for a 210 nm Si core thickness. ΔNRPS is very sensitive to the

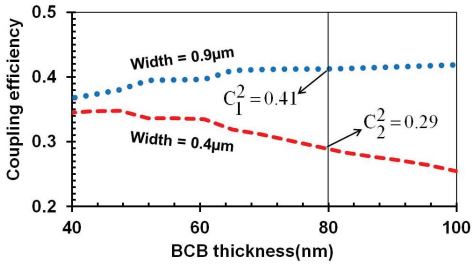

Fig. 3. Coupling efficiency in both arms of the MZI as a function of BCB thickness. $C_2^2/C_1^2 = 0.71$ for 80 nm of BCB thickness where C_1^2 and C_2^2 are the MMI power coupling coefficients of the broad (width = 0.9 μm) and narrow (width = 0.4 μm) arm, respectively.

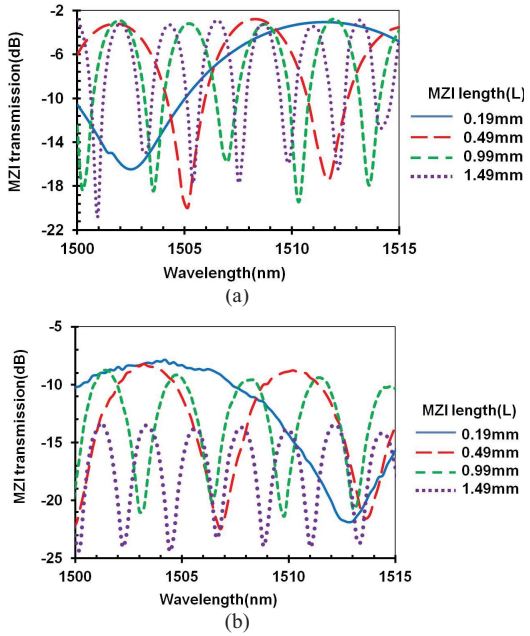

Fig. 4. Spectra of the MZIs for the 80 nm BCB thickness. (a) Simulated. (b) Experimentally measured.

silicon waveguide thickness. 210 nm thick Si core gives the optimum performance for the given waveguide widths of the MZI and Ce:YIG layer thickness.

III. Fabrication and Experimental Results

The details about the SOI photonic integrated circuit fabrication and bonding procedure can be found in [6] and [13], respectively. Curved diffraction gratings are used to inject the fundamental TM guided mode. In the magneto-optical measurements a stack of three 3 mm × 1 mm × 1 mm Nd-Fe-B permanent magnets are used to provide the required bias magnetic field for the Ce:YIG layer in the direction transverse to the light propagation. The optical transmission for forward and backward light propagation are recorded when an external unidirectional transverse magnetic field is applied. The magnetic field produced by the external magnet is sufficiently strong to saturate the Ce:YIG layer [5]. The simulated and experimentally measured spectra of the MZIs for various interferometer arm lengths (L) are depicted in Fig. 4(a) and Fig. 4(b), respectively for 80 nm BCB thickness. In MZI transmission simulations waveguide losses are not

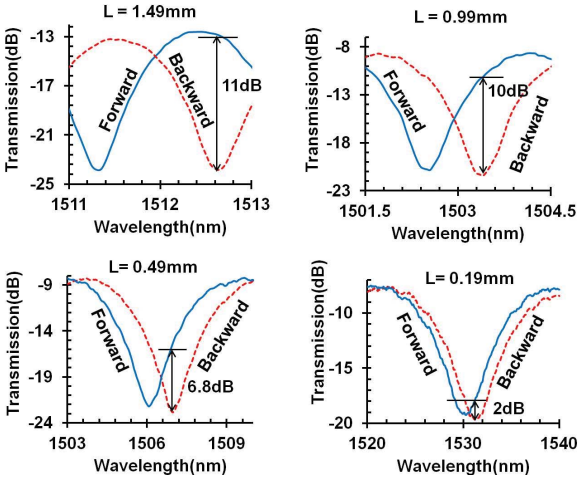

Fig. 5. Normalized transmission spectra for forward and backward light propagation in MZIs of different lengths.

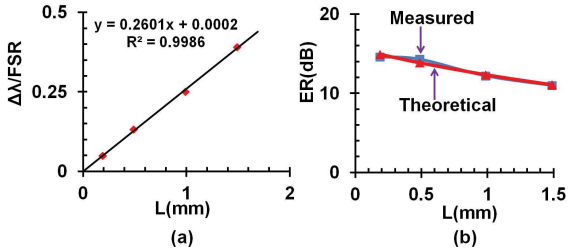

Fig. 6. (a) Measured $\Delta\lambda$/FSR for different arm lengths of the MZIs. (b) Fitting of measured extinction ratios for the different MZI lengths.

taken into account. The measured insertion loss of the MZI shown in Fig. 4(b) includes the overall propagation loss due to garnet bonded SOI plus transition loss at the junction between plain BCB covered SOI and garnet+BCB covered SOI. The obtained optical isolation from four devices with a respective Mach–Zehnder interferometer arm length L of 1.49 mm, 0.99 mm, 0.49 mm and 0.19 mm is presented in Fig. 5. The measured free spectral range of these devices is 2.3 nm, 3.4 nm, 6.8 nm and 18.4 nm, respectively whereas the simulated values are 2.3 nm, 3.3 nm, 6.6 nm and 18.3 nm, respectively from Fig. 4(a). The measured $\Delta\lambda$/FSR for different interferometer lengths is shown in Fig. 6(a), with $\Delta\lambda$ the difference in the wavelength for which destructive interference is obtained for the forward and backward direction. This ratio relates to the differential nonreciprocal phase shift per unit length as $\Delta\text{NRPS} = \Delta\lambda 2\pi/(\text{FSR} \times \text{L}) = 1.633$ rad/mm. Theoretically, the extinction ratio (ER) of a MZI with arm length L can be written as

$$ER = 20\log_{10}\left|\frac{1+(C_2/C_1)^2\exp(-\Delta\alpha L/2)}{1-(C_2/C_1)^2\exp(-\Delta\alpha L/2)}\right| \qquad (2)$$

where C_1^2 and C_2^2 are the MMI power coupling coefficients to the broad and narrow arm, respectively. $\Delta\alpha = \alpha_n - \alpha_b$ is the difference in propagation loss per unit length between the narrower and broader arm of the MZI. It is noteworthy here that (C_2/C_1) could be made equal to unity by redesigning the lateral positions of input and output waveguides of MMI which would lead to higher ER and hence higher isolation.

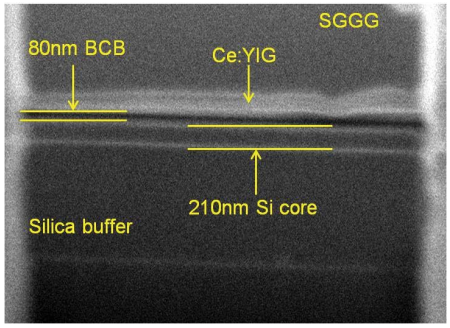

Fig. 7. SEM cross section of the bonded stack.

The measured extinction ratio for the four considered MZIs is shown in Fig. 6(b), together with the fitting of the theoretical extinction ratio. The fitting parameters are $(C_2/C_1)^2$ and $\Delta\alpha$. The different propagation loss in both arms is mostly due to the difference in optical confinement factor $\Delta\Gamma$ in the Ce:YIG layer. The composition of the sputtering target was $Ce_1Y_2Fe_5O_{12}$. The film was deposited by RF sputtering at 50 W power in Ar + O_2 (Ar: O_2 = 99:1, Ar = 6.2 sccm) ambience with substrate temperature of 690 °C. The deposition rate was around 2.2 nm/min. No annealing was applied after film deposition which leads to a high material loss of about 60 dB/cm compared to an annealed sample as reported in [14] having propagation loss of about 15 dB/cm. Taking the simulated value of $\Delta\Gamma$ as 0.07, $\Delta\alpha$ is evaluated theoretically as 0.42 dB/mm whereas the value obtained from the fit is 1.4 dB/mm. The difference between the theoretical and measured values can be partially explained by extra differential loss due to the confinement in the SGGG, which is assumed to be transparent in this analysis. The fitted value of $(C_2/C_1)^2$ is matched with the simulated one which is 0.71 as indicated in Fig. 3. Comparing the measured non-reciprocal phase shift with the simulation results presented in Fig. 2(b) results in a BCB thickness of 80 nm approximately, which is confirmed by a SEM cross-section as shown in Fig. 7.

IV. Conclusion

A very compact optical isolator on a silicon waveguide platform is realized by adhesive BCB bonding. The achieved isolation is 11 dB. While the device performance can be improved in terms of insertion loss and isolation ratio, this device concept allows for a dense co-integration of an optical isolator with semiconductor lasers on the SOI platform. This creates opportunities for the realization of complex active-passive photonic integrated circuits on a silicon platform.

References

[1] Y. Halioua, *et al.*, "Hybrid III–V semiconductor/silicon nanolaser," *Opt. Express*, vol. 19, no. 10, pp. 9221–9231, 2011.

[2] T. R. Zaman, X. Guo, and R. J. Ram, "Semiconductor waveguide isolators," *J. Lightw. Technol.*, vol. 26, no. 2, pp. 291–301, Jan. 15, 2008.

[3] H. Dötsch, *et al.*, "Application of magneto-optical waveguides in integrated optics: Review," *J. Opt. Soc. Amer.*, vol. 22, no. 1, pp. 240–253, 2005.

[4] Y. Shoji, *et al.*, "Magneto-optical isolator with silicon waveguides fabricated by direct bonding," *Appl. Phys. Lett.*, vol. 92, no. 7, pp. 071117-1–071117-3, 2008.

[5] M. C. Tien, T. Mizumoto, P. Pintus, H. Kromer, and J. E. Bowers, "Silicon ring isolators with bonded nonreciprocal magneto-optic garnets," *Opt. Express*, vol. 19, no. 12, pp. 11740–11745, 2011.

[6] S. Ghosh, S. Keyvavinia, W. Van Roy, T. Mizumoto, G. Roelkens, and R. Baets, "A Ce:YIG/silicon-on-insulator waveguide optical isolator realized by adhesive bonding," *Opt. Express*, vol. 20, no. 2, pp. 1839–1848, 2012.

[7] L. Bi, *et al.*, "On-chip optical isolation in monolithically integrated non-reciprocal optical resonators," *Nat. Photon.*, vol. 5, no. 12, pp. 758–762, 2011.

[8] Y. Yazaki, Y. Shoji, and T. Mizumoto, "Demonstration of interferometric waveguide isolator with a unidirectional magnetic field," *Jpn. J. Appl. Phys.*, vol. 46, pp. 5460–5464, Aug. 2007.

[9] S. Yamamoto and T. Makimoto, "Circuit theory for a class of anisotropic and gyrotropic thin-film optical waveguides and design of nonreciprocal devices for integrated optics," *J. Appl. Phys.*, vol. 45, no. 2, pp. 882–888, 1974.

[10] O. Zhuromskyy, *et al.*, "Analysis of polarization independent mach-zehnder-type integrated optical isolator," *J. Lightw. Technol.*, vol. 17, no. 7, pp. 1200–1205, Jul. 1999.

[11] *RSoft Design Group* [Online]. Available: http://www.rsoftdesign.com/

[12] D. Vermeulen, *et al.*, "Efficient tapering to the fundamental quasi-TM mode in asymmetrical waveguides," in *Proc. Eur. Conf. Integr. Opt.*, 2010, pp. 1–2.

[13] G. Roelkens, J. Brouckaert, D. Van Thourhout, R. Baets, R. Notzel, and M. Smit, "Adhesive bonding of InP/InGaAsP dies to processed silicon-on-insulator wafers using DVS-bis-benzocyclobutene," *J. Electrochem. Soc.*, vol. 153, no. 12, pp. G1015–G1019, Oct. 2006.

[14] T. Shintaku and T. Uno, "Preparation of Ce-substituted yttrium iron garnet films for magneto-optic waveguide devices," *Jpn. J. Appl. Phys.*, vol. 35, pp. 4689–4691, Sep. 1996.